Towards a Maximal Monotone Impact Law for Newton's Cradle

Tom Winandy, Remco I. Leine

Institute for Nonlinear Mechanics
University of Stuttgart
Pfaffenwaldring 9, D-70569 Stuttgart, Germany
[winandy, leine]@inm.uni-stuttgart.de

ABSTRACT

The 3-ball Newton's cradle is used as a stepping stone to divulge the structure of impact laws. A continuous cone-wise linear impact law which maps the pre-impact contact velocities to the post-impact contact velocities is proposed for the 3-ball Newton's cradle. The proposed impact law is kinematically, kinetically, and energetically consistent. It reproduces the outcomes of experimental observation. Moreover, it is in accordance with the outcome of the collision of three identical linear-elastic thin rods for which the impact process is governed by the one-dimensional wave equation. The proposed impact law is shown to be non-expansive. Therefore, the relationship between the mean contact velocity and its dual, the impulsive force, is maximal monotone. A counter-example to maximal cyclical monotonicity of this relationship allows to conclude that no dissipation function exists for the proposed impact law.

Keywords: Newton's cradle, unilateral constraints, impact, convex analysis, wave equation.

1 INTRODUCTION

In this paper, we present an impact law for Newton's cradle with 3 balls. We construct a continuous cone-wise linear impact law which is non-dissipative. The impact law provides the classical outcomes of the 3-ball Newton's cradle. The 3-ball Newton's cradle can be modelled as three identical linear-elastic thin rods which collide. The outcomes of the impact law are in accordance with the results of this model, which is governed by the one-dimensional wave equation.

Our aim is to divulge the structure of impact laws in order to be able to formulate maximal monotone impact laws for rigid multi-body systems that do not have the problems of existing impact laws such as kinematic, kinetic, and energetic inconsistency [1]. It is interesting to consider Newton's cradle because its phenomena cannot be described by the classical Newton's or Poisson's instantaneous impact law (see Figure 1(b)).

The impenetrability of unilateral constraints, which requires that the post-impact contact velocities γ_i^+ are non-negative, is referred to in this paper as kinematic consistency. In view of numerical integration, an impact-law should guarantee that arbitrary (also kinematically inadmissible) pre-impact contact velocities are mapped to kinematically admissible post-impact contact velocities.

Finally, we show that the impact law enjoys the maximal monotonicity property. The interest in the maximal monotonicity property stems from stability analysis and control of mechanical systems with unilateral constraints [2]. The maximal monotonicity property often allows the formulation of Lyapunov-based stability statements. In [3], the maximal monotonicity property is used for the design of state observers for unilaterally constrained multibody systems. Since the maximal monotonicity property implies dissipativity it might be a physically reasonable property for an impact law.

2 THE 3-BALL NEWTON'S CRADLE

The 3-ball Newton's cradle is shown in Figure 1(a). It consists of three balls of equal mass m with horizontal positions $\mathbf{q} = (q_1 \ q_2 \ q_3)^{\mathrm{T}}$ and velocities $\dot{\mathbf{q}} = \mathbf{u} = (u_1 \ u_2 \ u_3)^{\mathrm{T}}$. The contact distances are given by $\mathbf{g} = (q_2 - q_1 \ q_3 - q_2)^{\mathrm{T}}$. The unilateral constraint $\mathbf{g} \geq \mathbf{0}$ expresses the fact that contacts

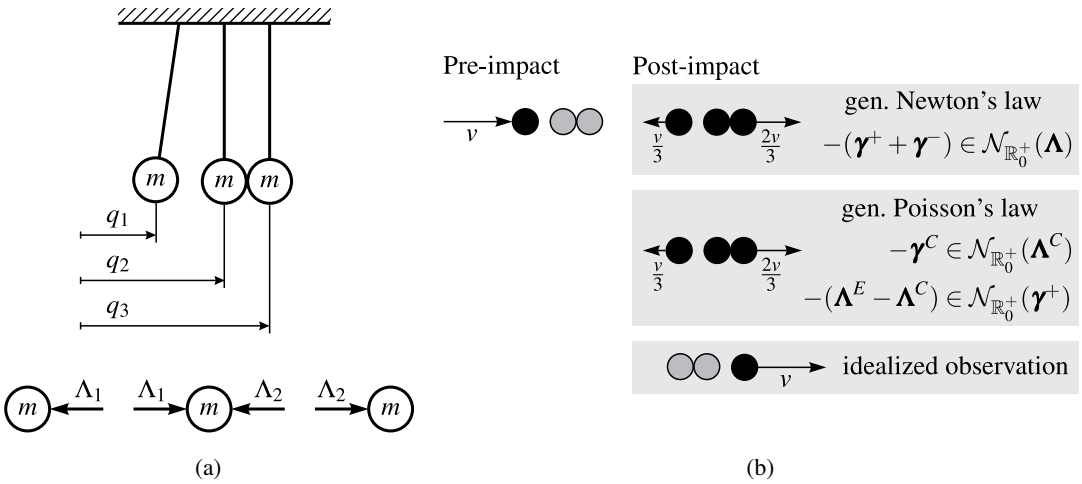

Figure 1. *Left:* Newton's cradle with 3 balls of mass *m*. *Right:* An example of outcomes by Newton's and Poisson's impact law.

can open but that the balls may not penetrate each other. The contact velocities are given by the relative velocities between the balls $\boldsymbol{\gamma} = (\gamma_1 \ \gamma_2)^{\mathrm{T}} = (u_2 - u_1 \ u_3 - u_2)^{\mathrm{T}}$. The pre- and post-impact velocities are designated by $\mathbf{u}^-$ and $\mathbf{u}^+$, respectively. Analogously, $\boldsymbol{\gamma}^-$ and $\boldsymbol{\gamma}^+$ designate the pre- and post-impact contact velocities.

The impact equations of the system can be written in the following matrix form

$$\mathbf{M}(\mathbf{u}^+ - \mathbf{u}^-) = \mathbf{W}\boldsymbol{\Lambda}, \tag{1}$$

$$\boldsymbol{\gamma}^{\pm} = \mathbf{W}^{\mathrm{T}}\mathbf{u}^{\pm}, \tag{2}$$

where $\boldsymbol{\Lambda} = (\Lambda_1 \ \Lambda_2)^{\mathrm{T}}$ are the impulsive contact forces during the impact. The impulsive force Λ_1 acts between balls 1 and 2, while Λ_2 occurs between balls 2 and 3. The matrix $\mathbf{W}$ is the matrix of generalized force directions for which holds $\mathbf{W}^{\mathrm{T}} = \frac{\partial \mathbf{g}}{\partial \mathbf{q}}$. For the 3-ball Newton's cradle, the mass matrix $\mathbf{M}$ and the matrix of generalized force directions $\mathbf{W}$ are

$$\mathbf{M} = \begin{pmatrix} m & 0 & 0 \\ 0 & m & 0 \\ 0 & 0 & m \end{pmatrix} \quad \text{and} \quad \mathbf{W} = \begin{pmatrix} -1 & 0 \\ 1 & -1 \\ 0 & 1 \end{pmatrix}. \tag{3}$$

The impact equation (1) needs to be complemented by an impact law that has the mathematical structure of a set-valued relationship [4]

$$-\boldsymbol{\Lambda} \in \mathcal{H}(\bar{\boldsymbol{\gamma}}), \tag{4}$$

where

$$\bar{\boldsymbol{\gamma}} = \frac{1}{2}\left(\boldsymbol{\gamma}^+ + \boldsymbol{\gamma}^-\right). \tag{5}$$

The operator $\mathcal{H}\colon \mathbb{R}^n \rightrightarrows \mathbb{R}^n$ is in general a set-valued operator. The combination of (1) and (2) yields the impact equation in contact velocities

$$\boldsymbol{\gamma}^+ - \boldsymbol{\gamma}^- = \mathbf{G}\boldsymbol{\Lambda} \quad \text{with} \quad \mathbf{G} := \mathbf{W}^{\mathrm{T}}\mathbf{M}^{-1}\mathbf{W}. \tag{6}$$

The matrix $\mathbf{G}$ is referred to as the Delassus operator.

Alternatively to the formulation as a set-valued relationship (4), the impact law can be expressed by a mapping S from pre- to post-impact contact velocities

$$\boldsymbol{\gamma}^+ = S(\boldsymbol{\gamma}^-), \tag{7}$$

or by a mapping Z from pre- to post-impact generalized velocities

$$\mathbf{u}^+ = Z(\mathbf{u}^-). \tag{8}$$

An impact law should be kinematically, kinetically, and energetically consistent:

- Pre-impact contact velocities $\boldsymbol{\gamma}^-$ and post-impact contact velocities $\boldsymbol{\gamma}^+$ are called *kinematically admissible* or *kinematically consistent* if

$$\boldsymbol{\gamma}^- \leq \mathbf{0} \quad \text{and} \quad \boldsymbol{\gamma}^+ \geq \mathbf{0}, \tag{9}$$

  respectively.

- *Kinetic consistency* is required by the unilateral character of non-adhesive contacts which requires the contact forces to be non-negative

$$\boldsymbol{\Lambda} \geq \mathbf{0}. \tag{10}$$

  The contact force vanishes if the contact is open, i.e. if $\mathbf{g} > \mathbf{0}$. If $\mathbf{g} = \mathbf{0}$ the contact is closed and it can only transfer non-negative contact forces.

- *Energetic consistency* means that there is no increase in energy during the impact. Let the kinetic energy before and after the impact be designated by $T^- = \frac{1}{2}\mathbf{u}^{-\mathrm{T}}\mathbf{M}\mathbf{u}^-$ and $T^+ = \frac{1}{2}\mathbf{u}^{+\mathrm{T}}\mathbf{M}\mathbf{u}^+$, respectively. Energetic consistency then requires that

$$T^+ \leq T^- \Leftrightarrow T^+ - T^- \leq 0, \tag{11}$$

  which can be expressed in terms of pre- and post impact velocities

$$\mathbf{u}^{+\mathrm{T}}\mathbf{M}\mathbf{u}^+ - \mathbf{u}^{-\mathrm{T}}\mathbf{M}\mathbf{u}^- = \left(\mathbf{u}^+ + \mathbf{u}^-\right)^{\mathrm{T}}\mathbf{M}\left(\mathbf{u}^+ - \mathbf{u}^-\right) \leq 0. \tag{12}$$

  The use of (1), (2), and (6) permits to rewrite (12) as

$$\left(\boldsymbol{\gamma}^+ + \boldsymbol{\gamma}^-\right)^{\mathrm{T}}\mathbf{G}^{-1}\left(\boldsymbol{\gamma}^+ - \boldsymbol{\gamma}^-\right) = \boldsymbol{\gamma}^{+\mathrm{T}}\mathbf{G}^{-1}\boldsymbol{\gamma}^+ - \boldsymbol{\gamma}^{-\mathrm{T}}\mathbf{G}^{-1}\boldsymbol{\gamma}^- \leq 0. \tag{13}$$

  The conditions (12) and (13) for energetic consistency can be expressed using the norms with metric $\mathbf{M}$ and $\mathbf{G}^{-1}$, respectively

$$\|\mathbf{u}^+\|^2_{\mathbf{M}} \leq \|\mathbf{u}^-\|^2_{\mathbf{M}} \quad \text{and} \quad \|\boldsymbol{\gamma}^+\|^2_{\mathbf{G}^{-1}} \leq \|\boldsymbol{\gamma}^-\|^2_{\mathbf{G}^{-1}}. \tag{14}$$

From [5, 4], it is known that the maximal monotonicity of the operator $\mathcal{H}$ in (4) is equivalent to non-expansivity properties of the impact mappings (7) and (8).

Definition 1 (Maximal monotonicity [5])**.** *A mapping $\mathcal{T}\colon \mathbb{R}^n \rightrightarrows \mathbb{R}^n$ is called monotone if it has the property that*

$$(\boldsymbol{y}_A - \boldsymbol{y}_B)^{\mathrm{T}}(\boldsymbol{x}_A - \boldsymbol{x}_B) \geq 0, \tag{15}$$

whenever $\boldsymbol{y}_A \in \mathcal{T}(\boldsymbol{x}_A)$, $\boldsymbol{y}_B \in \mathcal{T}(\boldsymbol{x}_B)$. Moreover, $\mathcal{T}$ is called maximal monotone if it is monotone and its graph cannot be enlarged without destroying this property.

Definition 2 (Non-expansivity [5, 4])**.** *A mapping $\mathcal{F}\colon \mathbb{R}^n \rightrightarrows \mathbb{R}^n$ is called non-expansive in the metric $\mathbf{P}$ if it has the property that*

$$\|\boldsymbol{y}_A - \boldsymbol{y}_B\|_{\mathbf{P}} \leq \|\boldsymbol{x}_A - \boldsymbol{x}_B\|_{\mathbf{P}}, \tag{16}$$

whenever $\boldsymbol{y}_A \in \mathcal{F}(\boldsymbol{x}_A)$, $\boldsymbol{y}_B \in \mathcal{F}(\boldsymbol{x}_B)$.

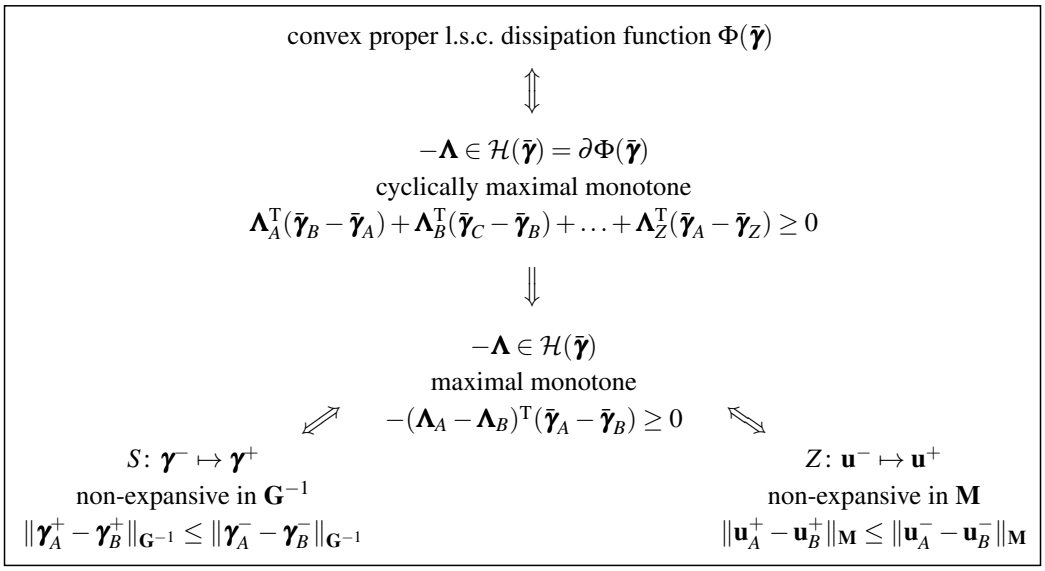

Figure 2. Interrelations of a maximal monotone impact law [4].

Furthermore, the set-valued operator $\mathcal{H}$ can be written as the subdifferential to a convex proper lower semicontinuous (l.s.c.) dissipation function Φ such that

$$-\boldsymbol{\Lambda} \in \mathcal{H}(\bar{\boldsymbol{\gamma}}) = \partial\Phi(\bar{\gamma}), \tag{17}$$

if and only if $\mathcal{H}$ is maximal cyclically monotone.

Definition 3 (Cyclical monotonicity [5])**.** *A mapping $\mathcal{T}\colon \mathbb{R}^n \rightrightarrows \mathbb{R}^n$ is cyclically monotone if for any cycle of m points $\boldsymbol{x}_A, \boldsymbol{x}_B, \ldots, \boldsymbol{x}_Z$ (for arbitrary $m \geq 2$) and elements $\mathbf{y}_i \in \mathcal{T}(\boldsymbol{x}_i)$, one has*

$$\boldsymbol{y}_A^{\mathrm{T}}(\boldsymbol{x}_B - \boldsymbol{x}_A) + \boldsymbol{y}_B^{\mathrm{T}}(\boldsymbol{x}_C - \boldsymbol{x}_B) + \ldots + \boldsymbol{y}_Z^{\mathrm{T}}(\boldsymbol{x}_A - \boldsymbol{x}_Z) \leq 0. \tag{18}$$

It is maximal cyclically monotone if it is cyclically monotone and its graph cannot be enlarged without destroying this property.

Note that cyclical monotonicity is a stronger condition than monotonicity. Definition 3 reduces to Definition 1 when $m = 2$. The relations between the non-expansivity and monotonicity properties are shown in Figure 2.

3 THE SEQUENTIAL IMPACT LAW

We propose a continuous cone-wise linear impact mapping $S\colon \mathbb{R}^2 \to \mathbb{R}^2,\ \boldsymbol{\gamma}^- \mapsto \boldsymbol{\gamma}^+$ for the 3-ball Newton's cradle. The impact mapping S takes the form

$$\boldsymbol{\gamma}^+ = S(\boldsymbol{\gamma}^-) = \mathbf{Q}_i \boldsymbol{\gamma}^-, \tag{19}$$

where $\mathbf{Q}_i \in \mathbb{R}^{2\times 2}$ are 2-by-2 matrices which apply in a corresponding cone in the (γ_1^-, γ_2^-)-plane. We construct the matrices $\mathbf{Q}_i$ together with their respective cones C_i by demanding the following properties of the impact law:

- **P1** The mapping is continuous, i.e. $\mathbf{Q}_i \mathbf{v}_i = \mathbf{Q}_{i+1}\mathbf{v}_i$ with $\mathbf{v}_i$ being the direction of the boundary half-line between the cones C_i and C_{i+1}.
- **P2** Conservation of energy holds, i.e. $\|\boldsymbol{\gamma}^+\|_{\mathbf{G}^{-1}} = \|\mathbf{Q}_i\boldsymbol{\gamma}^-\|_{\mathbf{G}^{-1}} = \|\boldsymbol{\gamma}^-\|_{\mathbf{G}^{-1}}$ for all matrices $\mathbf{Q}_i$. This implies energetic consistency.
- **P3** Each cone $\mathbf{Q}_i$ is mapped to the entire first quadrant, i.e. the cone C_i is spanned by the columns of $\mathbf{Q}_i^{-1}$. This implies kinematic consistency.

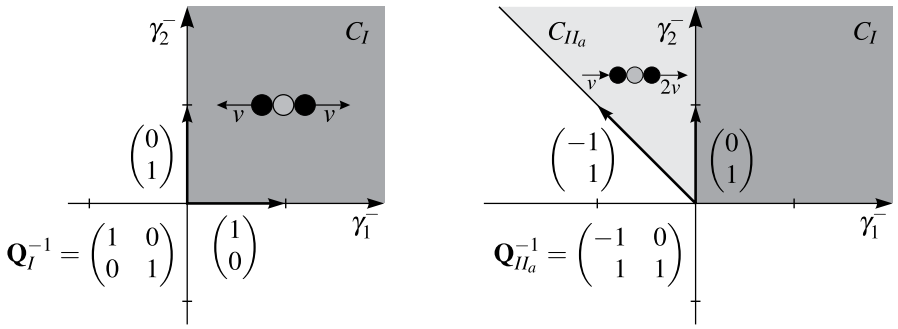

(a) Cone C_I (b) Cone C_{II_a}

Figure 3. Construction steps of the impact mapping S.

We start with the first quadrant (see Figure 3(a)). Pre-impact contact velocities from the first quadrant are positive which means that no impact occurs. Therefore, we set

$$\mathbf{Q}_I = \begin{pmatrix}1 & 0\\0 & 1\end{pmatrix}, \tag{20}$$

which means that $\boldsymbol{\gamma}^+ = \boldsymbol{\gamma}^-$ for all $\boldsymbol{\gamma}^- \in C_I$. The cone C_I is spanned by the columns of $\mathbf{Q}_I^{-1}$.

Next, we proceed to the cone C_{II_a} on the left of C_I as shown in Figure 3(b). The boundary between the two cones is given by the positive γ_2^--axis. Continuity and conservation of energy (**P1** and **P2**) lead us to the matrix

$$\mathbf{Q}_{II_a} = \begin{pmatrix}-1 & 0\\1 & 1\end{pmatrix}. \tag{21}$$

The direction of the boundary to the next cone can be read from $\mathbf{Q}_{II_a}^{-1}$ (**P3**) as it is shown in Figure 3(b), such that

$$\mathbf{v}_{II_a} = \begin{pmatrix}-1\\1\end{pmatrix}. \tag{22}$$

We can proceed analogously to find all six cones C_i with $i \in \{I, II_a, II_b, III, IV_a, IV_b\}$ together with their corresponding matrices

$$\begin{aligned}
\mathbf{Q}_I &= \begin{pmatrix}1 & 0\\0 & 1\end{pmatrix}, \qquad \mathbf{Q}_{II_a} = \begin{pmatrix}-1 & 0\\1 & 1\end{pmatrix}, \quad \mathbf{Q}_{II_b} = \begin{pmatrix}0 & 1\\-1 & -1\end{pmatrix},\\
\mathbf{Q}_{III} &= \begin{pmatrix}0 & -1\\-1 & 0\end{pmatrix}, \quad \mathbf{Q}_{IV_a} = \begin{pmatrix}1 & 1\\0 & -1\end{pmatrix}, \quad \mathbf{Q}_{IV_b} = \begin{pmatrix}-1 & -1\\1 & 0\end{pmatrix}.
\end{aligned} \tag{23}$$

The repartition of the (γ_1^-, γ_2^-)-plane into the six cones C_i with $i \in \{I, II_a, II_b, III, IV_a, IV_b\}$ is depicted in Figure 4(a). The symmetry of the problem appears in the symmetry between the matrices $\mathbf{Q}_{II_a}$ and $\mathbf{Q}_{IV_a}$ as well as between $\mathbf{Q}_{II_b}$ and $\mathbf{Q}_{IV_b}$.

In the following, we will call the impact law (19) the *Sequential Impact Law* because it is equivalent to a sequence of impacts between only two balls. This can be seen by the following properties

$$\begin{aligned}
\mathbf{Q}_{II_b} &= \mathbf{Q}_{IV_a}\mathbf{Q}_{II_a},\\
\mathbf{Q}_{IV_b} &= \mathbf{Q}_{II_a}\mathbf{Q}_{IV_a},\\
\mathbf{Q}_{III} &= \mathbf{Q}_{IV_a}\mathbf{Q}_{II_a}\mathbf{Q}_{IV_a} = \mathbf{Q}_{II_a}\mathbf{Q}_{IV_a}\mathbf{Q}_{II_a},
\end{aligned} \tag{24}$$

where $\mathbf{Q}_{II_a}$ and $\mathbf{Q}_{IV_a}$ describe the impact between only two of the three balls as will be shown below.

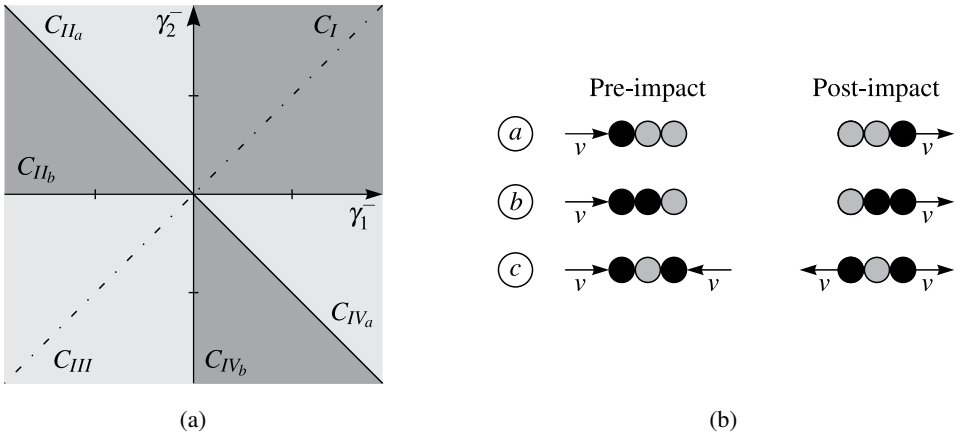

(a) (b)

Figure 4. *Left:* The different cones in the (γ_1^-, γ_2^-)-plane. The dot-dashed line marks the symmetry line. *Right:* Idealized observations.

After having derived the Sequential Impact Law, we want to argue why it is a reasonable choice. In the following, the implications of the Sequential Impact Law are discussed for the four quadrants of the (γ_1^-, γ_2^-)-plane.

The first quadrant is equal to the cone C_I and it corresponds to two positive pre-impact contact velocities such that no impact happens. The identity map is the only reasonable choice for the first quadrant.

The third quadrant is equal to the cone C_{III} and it corresponds to both pre-impact contact velocities being negative and therefore kinematically admissible. Hence, the third quadrant contains all the classical experimental outcomes which can be realized with a 3-ball Newton's cradle. Figure 4(b) gives three examples of idealized observations from cone C_{III}. The Sequential Impact Law provides these idealized experimental outcomes.

The second and the fourth quadrant correspond to one pre-impact contact velocity being positive and the other being negative. Each one of these quadrants contains two different cones, because the magnitude of the positive pre-impact contact velocity determines whether the corresponding outer ball participates in the impact process or not. The cones C_{II_a} and C_{IV_a}, which are adjacent to the first quadrant, correspond to a single impact between only two of the three balls. In the cone C_{II_a}, the right ball does not participate in the impact process because it has a positive pre-impact contact velocity that prevents it from colliding with the middle ball. This can be seen by considering the impact equation in the contact velocities (6) and the Sequential Impact Law (19) for pre-impact velocities $\boldsymbol{\gamma}^- \in C_{II_a}$

$$\boldsymbol{\gamma}^+ - \boldsymbol{\gamma}^- = (\mathbf{Q}_{II_a} - \mathbf{I})\boldsymbol{\gamma}^- = \mathbf{G}\boldsymbol{\Lambda}, \tag{25}$$

where $\mathbf{I}$ denotes the identity matrix. Eq. (25) yields the impulsive force

$$\boldsymbol{\Lambda} = \begin{pmatrix} -m\gamma_1^- \\ 0 \end{pmatrix}, \tag{26}$$

from which it becomes apparent that the right ball does not participate in the impact process. In C_{IV_a}, it is the left ball that is not subjected to any impact. For pre-impact velocities belonging to the cones C_{II_a} and C_{IV_a}, the Sequential Impact Law provides the same result as it is given by the generalized Newton and by the generalized Poisson impact law for the non-dissipative impact of two balls [6, 7]. The positive pre-impact contact velocity in the cones C_{II_b} and C_{IV_b} does not prevent the interaction between the three balls through wave effects.

The third quadrant basically completely describes the physics of Newton's cradle as it covers all physically realizable experiments with Newton's cradle. Nevertheless, the first, the second, and the

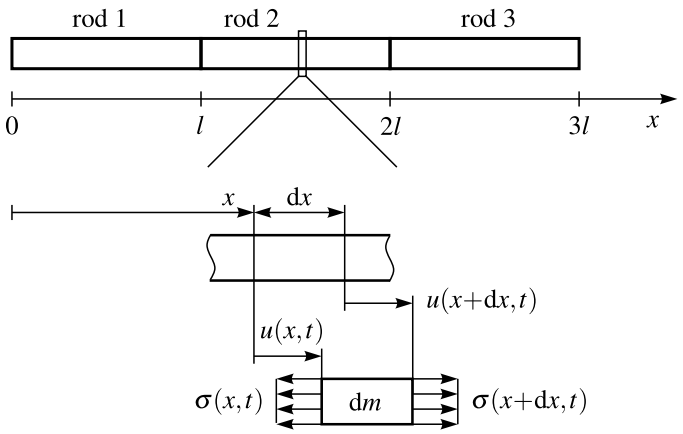

Figure 5. Collision of 3 identical thin rods. The lower part shows the stresses acting on a differential element of the rod.

fourth quadrant are needed to deal with kinematically inadmissible pre-impact contact velocities, which is important in view of numerical simulation. Small numerical errors may lead to positive pre-impact contact velocities and an impact law should map these pre-impact contact velocities to physically reasonable post-impact contact velocities.

In the next section, we provide a further argument for the validity of the Sequential Impact Law by showing that it provides the same outcomes as the one-dimensional wave equation does for the collision of three identical thin rods.

4 THIN ROD MODEL OF THE 3-BALL NEWTON'S CRADLE

Wave effects play a crucial role in the impact process of the 3-ball Newton's cradle. We model the system with three identical thin rods (see Figure 5). This leads us to a description of the impact process that is governed by the one-dimensional wave equation.

The rods have cross-section A and density ρ. We consider the stresses acting on a differential element of the rod as it is shown in Figure 5. The position of the differential element is denoted by x. The displacement field is referred to as $u(x,t)$. The balance of linear momentum in x direction for the differential element is then given by

$$\mathrm{d}m\, u_{tt}(x,t) = A\left(\sigma(x+\mathrm{d}x,t) - \sigma(x,t)\right). \tag{27}$$

The mass element $\mathrm{d}m$ can be expressed in terms of $\mathrm{d}x$ as

$$\mathrm{d}m = \rho A \mathrm{d}x. \tag{28}$$

Further, we assume that the rods behave linear-elastically and thus obey Hooke's law

$$\sigma = E\varepsilon = E u_x, \tag{29}$$

where E and ε designate the Young's modulus and the strain, respectively. Using (28) and (29), we can rewrite (27) as

$$\rho A \mathrm{d}x\, u_{tt}(x,t) = AE\left(u_x(x+\mathrm{d}x,t) - u_x(x,t)\right). \tag{30}$$

Dividing (30) by $\rho A \mathrm{d}x$ and letting $\mathrm{d}x \to 0$ yields the classical one-dimensional wave equation

$$u_{tt}(x,t) = c^2 u_{xx}(x,t) \quad \text{with} \quad c^2 = \frac{E}{\rho}, \tag{31}$$

where c denotes the propagation velocity of longitudinal waves in the rod.

Table 1. Transition properties of longitudinal waves in thin rods.

Type	Diagram	Transition conditions
Free end	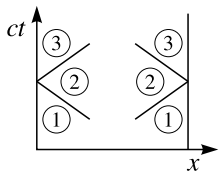	$u_{1,x} = 0$ $u_{3,x} = 0$ $u_{1,t} + u_{3,t} = 2u_{2,t}$
Impact between ends	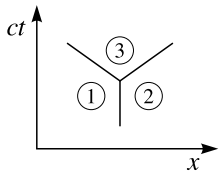	$u_{3,x} = \frac{1}{2c}(u_{2,t} - u_{1,t})$ $u_{3,t} = \frac{1}{2}(u_{2,t} + u_{1,t})$
Crossing waves	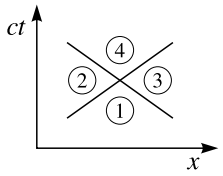	$u_{1,x} + u_{4,x} = u_{2,x} + u_{3,x}$ $u_{1,t} + u_{4,t} = u_{2,t} + u_{3,t}$

Our aim is to investigate the impact effects in Newton's cradle by considering colliding rods. An impact between two colliding rods leads to discontinuities in the velocity and in the strain which expand through the colliding rods with velocity c. These discontinuities can only propagate along characteristics of the solution of the wave equation (31). The construction of a characteristics diagram provides a way to investigate the wave propagation process. Detailed information about waves in elastic solids can be found in [8, 9]. In order to be able to construct characteristics diagrams, we first summarize some transition conditions of the longitudinal waves in Table 1.

4.1 Collision of two identical thin rods

We consider the collision of two identical thin rods. Before the impact, both rods are undeformed. Initially, the left rod has a uniform velocity v while the right rod is at rest. We assume that the colliding ends of the rods have the same velocity as soon as they touch. The pre-impact configuration can be seen in Figure 6(a). The initial conditions can be stated as

$$\begin{aligned} u_x(x,0) &= 0 \quad \text{if } x \in [0,2l], \\ u_t(x,0) &= \begin{cases} v & \text{if } x \in [0,l], \\ 0 & \text{if } x \in (l,2l]. \end{cases} \end{aligned} \tag{32}$$

Discontinuities in the velocity and in the strain can only propagate along their characteristics. These characteristics of the wave equation (31) delimit regions inside which the strains and the velocities are constant. Therefore, we state the strain and velocity for each region in the characteristics diagram in Figure 6(a). The transition properties from Table 1 allow the construction of the characteristics diagram and the calculation of the corresponding strains and velocities which are prevalent in the different regions in the characteristics diagram

$$\begin{aligned} &\text{Region } ①: \quad u_{1,x} = 0, && u_{1,t} = v, \\ &\text{Region } ②: \quad u_{2,x} = 0, && u_{2,t} = 0, \\ &\text{Region } ③: \quad u_{3,x} = -\frac{v}{2c}, && u_{3,t} = \frac{v}{2}, \\ &\text{Region } ④: \quad u_{4,x} = 0, && u_{4,t} = 0, \\ &\text{Region } ⑤: \quad u_{5,x} = 0, && u_{5,t} = v. \end{aligned} \tag{33}$$

In A, the contact opens, the left rod is at rest and the right rod has the uniform velocity v.

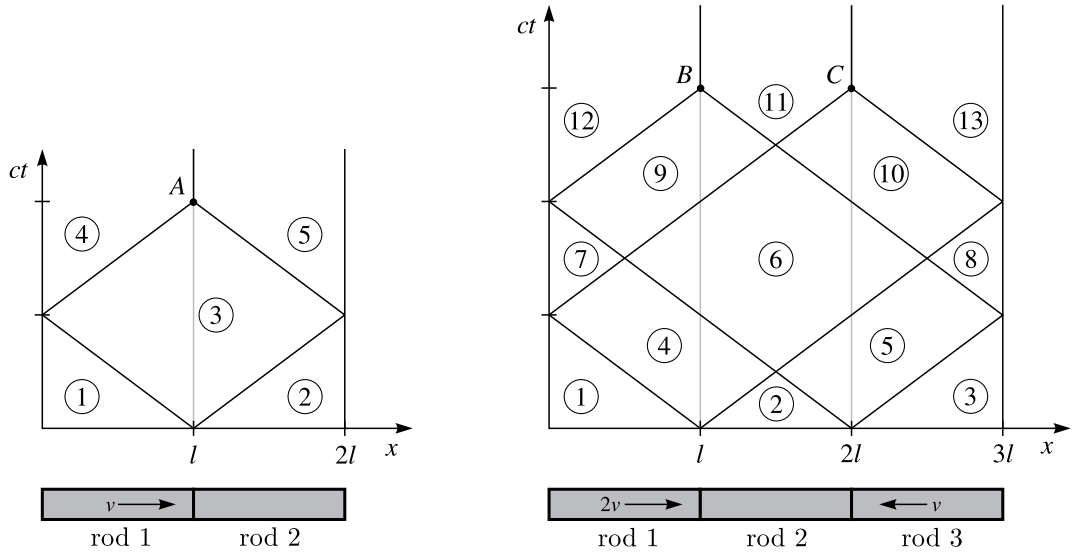

(a) Two rods (b) Three rods

Figure 6. Characteristics diagrams for colliding identical thin rods.

We can conclude that the collision of two identical thin rods leads to the same result as Newton's and Poisson's impact law do for two balls in the non-dissipative case. Moreover, the Sequential Impact Law also provides this outcome in the cones C_{II_a} and C_{IV_a} which correspond to the present situation of a single impact between two balls.

4.2 Collision of three identical thin rods

We now consider three identical thin rods. Initially, the middle rod is at rest. It is approached by the left and by the right rod which have velocities $2v$ and $-v$, respectively. Again, the rods are undeformed before the collision. The initial conditions can be written as

$$u_x(x,0) = 0 \quad \text{if } x \in [0,3l],$$
$$u_t(x,0) = \begin{cases} 2v & \text{if } x \in [0,l], \\ 0 & \text{if } x \in (l,2l], \\ -v & \text{if } x \in (2l,3l]. \end{cases} \tag{34}$$

As in the previous case, we assume that the colliding ends of the rods have the same velocity as soon as they touch. Again, a characteristics diagram is constructed (see Figure 6(b)) using the transition properties from Table 1. The following velocities and strains are obtained for the different regions in the diagram

$$\begin{array}{llll}
\text{Region } ①: & u_{1,x} = 0, & u_{1,t} = 2v, & \\
\text{Region } ②: & u_{2,x} = 0, & u_{2,t} = 0, & \\
\text{Region } ③: & u_{3,x} = 0, & u_{3,t} = -v, & \\
\text{Region } ④: & u_{4,x} = -\dfrac{v}{c}, & u_{4,t} = v, & \\
\text{Region } ⑤: & u_{5,x} = -\dfrac{v}{2c}, & u_{5,t} = -\dfrac{v}{2}, & \\
\text{Region } ⑥: & u_{6,x} = -\dfrac{3v}{2c}, & u_{6,t} = \dfrac{v}{2}, & \\
\text{Region } ⑦: & u_{7,x} = 0, & u_{7,t} = 0, & \\
\text{Region } ⑧: & u_{8,x} = 0, & u_{8,t} = 0, & \\
\text{Region } ⑨: & u_{9,x} = -\dfrac{v}{2c}, & u_{9,t} = -\dfrac{v}{2}, & \\
\text{Region } ⑩: & u_{10,x} = -\dfrac{v}{c}, & u_{10,t} = v, & \\
\text{Region } ⑪: & u_{11,x} = 0, & u_{11,t} = 0, & \\
\text{Region } ⑫: & u_{12,x} = 0, & u_{12,t} = -v, & \\
\text{Region } ⑬: & u_{13,x} = 0, & u_{13,t} = 2v. &
\end{array} \tag{35}$$

In B and C, both contacts open simultaneously. The left rod has a post-impact velocity of v. The middle rod is at rest and the right rod has a post-impact velocity of $2v$. This corresponds exactly to the outcome which is provided by the Sequential Impact Law as can be seen by calculating the pre- and post-impact relative velocities of the rods

$$\boldsymbol{\gamma}^- = \begin{pmatrix} -2v \\ -v \end{pmatrix} \quad \text{and} \quad \boldsymbol{\gamma}^+ = \begin{pmatrix} v \\ 2v \end{pmatrix}, \tag{36}$$

for which indeed holds $\boldsymbol{\gamma}^+ = S(\boldsymbol{\gamma}^-) = \mathbf{Q}_{III}\boldsymbol{\gamma}^-$. Note that Newton's and Poisson's instantaneous impact law would give a different outcome.

5 CONTRACTION PROPERTIES OF THE SEQUENTIAL IMPACT LAW

Since we are interested in the mathematical structure of impact laws, we investigate which properties from Figure 2 hold for the Sequential Impact Law.

5.1 Non-expansivity of the Sequential Impact Law

In the following, we show that the Sequential Impact Law is non-expansive in the metric $\mathbf{G}^{-1}$. This means that the set-valued relationship (4) between the dual variables $\bar{\boldsymbol{\gamma}}$ and $\boldsymbol{\Lambda}$ is maximal monotone.

Theorem 1. *The impact mapping* (19) *is non-expansive in the metric* $\mathbf{G}^{-1}$*, i.e.*

$$\|\boldsymbol{\gamma}_A^+ - \boldsymbol{\gamma}_B^+\|_{\mathbf{G}^{-1}} \leq \|\boldsymbol{\gamma}_A^- - \boldsymbol{\gamma}_B^-\|_{\mathbf{G}^{-1}} \quad \forall \boldsymbol{\gamma}_A^-, \boldsymbol{\gamma}_B^- \in \mathbb{R}^2. \tag{37}$$

Proof. The condition (37) needs to hold for arbitrary pairs of pre-impact contact velocities $\boldsymbol{\gamma}_A^-$ and $\boldsymbol{\gamma}_B^-$. The idea behind the proof is to decompose the line that connects the points $\boldsymbol{\gamma}_A^-$ and $\boldsymbol{\gamma}_B^-$ into a series of segments which lie in a single cone respectively. This decomposition can be done using telescopic expansion

$$\|\boldsymbol{\gamma}_A^+ - \boldsymbol{\gamma}_B^+\|_{\mathbf{G}^{-1}} = \|\boldsymbol{\gamma}_A^+ - \boldsymbol{\gamma}_{*1}^+ + \boldsymbol{\gamma}_{*1}^+ - \boldsymbol{\gamma}_{*2}^+ + \ldots + \boldsymbol{\gamma}_{*k}^+ - \boldsymbol{\gamma}_B^+\|_{\mathbf{G}^{-1}}, \tag{38}$$

where the $\boldsymbol{\gamma}_{*i}^+$ are the images of $\boldsymbol{\gamma}_{*i}^-$ which lie on the boundaries between the cones. Figure 7(a) shows an example of this decomposition. At the boundary between the cones C_i and C_{i+1}, we have that $\boldsymbol{\gamma}_{*i}^+ = \mathbf{Q}_i\boldsymbol{\gamma}_{*i}^- = \mathbf{Q}_{i+1}\boldsymbol{\gamma}_{*i}^-$ due to continuity (**P1**). Therefore, eq. (38) can be written as

$$\|\boldsymbol{\gamma}_A^+ - \boldsymbol{\gamma}_B^+\|_{\mathbf{G}^{-1}} = \|\mathbf{Q}_A(\boldsymbol{\gamma}_A^- - \boldsymbol{\gamma}_{*1}^-) + \mathbf{Q}_1(\boldsymbol{\gamma}_{*1}^- - \boldsymbol{\gamma}_{*2}^-) + \ldots + \mathbf{Q}_B(\boldsymbol{\gamma}_{*k}^- - \boldsymbol{\gamma}_B^-)\|_{\mathbf{G}^{-1}}. \tag{39}$$

From the triangle inequality, it follows that

$$\begin{aligned} \|\boldsymbol{\gamma}_A^+ - \boldsymbol{\gamma}_B^+\|_{\mathbf{G}^{-1}} &= \|\mathbf{Q}_A(\boldsymbol{\gamma}_A^- - \boldsymbol{\gamma}_{*1}^-) + \mathbf{Q}_1(\boldsymbol{\gamma}_{*1}^- - \boldsymbol{\gamma}_{*2}^-) + \ldots + \mathbf{Q}_B(\boldsymbol{\gamma}_{*k}^- - \boldsymbol{\gamma}_B^-)\|_{\mathbf{G}^{-1}} \\ &\leq \|\mathbf{Q}_A(\boldsymbol{\gamma}_A^- - \boldsymbol{\gamma}_{*1}^-)\|_{\mathbf{G}^{-1}} + \|\mathbf{Q}_1(\boldsymbol{\gamma}_{*1}^- - \boldsymbol{\gamma}_{*2}^-)\|_{\mathbf{G}^{-1}} + \ldots + \|\mathbf{Q}_B(\boldsymbol{\gamma}_{*k}^- - \boldsymbol{\gamma}_B^-)\|_{\mathbf{G}^{-1}}. \end{aligned} \tag{40}$$

Due to the energy conservation property **P2**, it holds that $\|\mathbf{Q}_i\boldsymbol{\gamma}^-\|_{\mathbf{G}^{-1}} = \|\boldsymbol{\gamma}^-\|_{\mathbf{G}^{-1}}$. This leads to

$$\|\boldsymbol{\gamma}_A^+ - \boldsymbol{\gamma}_B^+\|_{\mathbf{G}^{-1}} \leq \|\boldsymbol{\gamma}_A^- - \boldsymbol{\gamma}_{*1}^-\|_{\mathbf{G}^{-1}} + \|\boldsymbol{\gamma}_{*1}^- - \boldsymbol{\gamma}_{*2}^-\|_{\mathbf{G}^{-1}} + \ldots + \|\boldsymbol{\gamma}_{*k}^- - \boldsymbol{\gamma}_B^-\|_{\mathbf{G}^{-1}}. \tag{41}$$

Each $\boldsymbol{\gamma}_{*i}^-$ can be expressed in terms of $\boldsymbol{\gamma}_A^-$ and $\boldsymbol{\gamma}_B^-$ as the convex combination

$$\boldsymbol{\gamma}_{*i}^- = \alpha_i\boldsymbol{\gamma}_A^- + (1-\alpha_i)\boldsymbol{\gamma}_B^- \quad \text{with} \;\; \alpha_i \in [0,1]. \tag{42}$$

Eq. (42) allows to rewrite the terms of the right-hand side of (41) in the following way

$$\begin{aligned} \|\boldsymbol{\gamma}_A^- - \boldsymbol{\gamma}_{*1}^-\|_{\mathbf{G}^{-1}} &= (1-\alpha_1)\|\boldsymbol{\gamma}_A^- - \boldsymbol{\gamma}_B^-\|_{\mathbf{G}^{-1}}, \\ \|\boldsymbol{\gamma}_{*1}^- - \boldsymbol{\gamma}_{*2}^-\|_{\mathbf{G}^{-1}} &= (\alpha_1 - \alpha_2)\|\boldsymbol{\gamma}_A^- - \boldsymbol{\gamma}_B^-\|_{\mathbf{G}^{-1}}, \\ &\vdots \\ \|\boldsymbol{\gamma}_{*k}^- - \boldsymbol{\gamma}_B^-\|_{\mathbf{G}^{-1}} &= \alpha_k\|\boldsymbol{\gamma}_{*k}^- - \boldsymbol{\gamma}_B^-\|_{\mathbf{G}^{-1}}. \end{aligned} \tag{43}$$

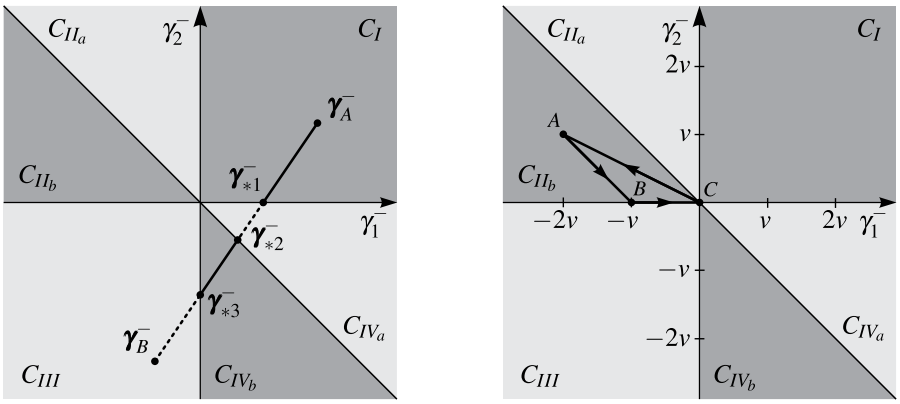

Figure 7. *Left:* Exemplary decomposition of the path between $\boldsymbol{\gamma}_A^-$ and $\boldsymbol{\gamma}_B^-$. *Right: ABC*-cycle which provides a counter-example to the maximal cyclical monotonicity of the impact mapping S.

Finally, we use the expressions from (43) to rewrite (41) as

$$\begin{aligned}\|\boldsymbol{\gamma}_A^+ - \boldsymbol{\gamma}_B^+\|_{\mathbf{G}^{-1}} \leq (1-\alpha_1)\|\boldsymbol{\gamma}_A^- - \boldsymbol{\gamma}_B^-\|_{\mathbf{G}^{-1}} + (\alpha_1-\alpha_2)\|\boldsymbol{\gamma}_A^- - \boldsymbol{\gamma}_B^-\|_{\mathbf{G}^{-1}} + \dots \\ + \alpha_k\|\boldsymbol{\gamma}_{*k}^- - \boldsymbol{\gamma}_B^-\|_{\mathbf{G}^{-1}} \\ = \|\boldsymbol{\gamma}_A^- - \boldsymbol{\gamma}_B^-\|_{\mathbf{G}^{-1}},\end{aligned} \tag{44}$$

which completes the proof. □

5.2 A counter-example to maximal cyclical monotonicity

In order to give a counter-example to the maximal cyclical monotonicity of (4), we propose to consider an *ABC*-cycle which leads to a contradiction to inequality (18) in Definition 3. We consider the following *ABC*-cycle of pre-impact contact velocities

$$\boldsymbol{\gamma}_A^- = \begin{pmatrix}-2v & v\end{pmatrix}^{\mathrm{T}}, \qquad \boldsymbol{\gamma}_B^- = \begin{pmatrix}-v & 0\end{pmatrix}^{\mathrm{T}}, \qquad \boldsymbol{\gamma}_C^- = \begin{pmatrix}0 & 0\end{pmatrix}^{\mathrm{T}}. \tag{45}$$

The cycle of pre-impact contact velocities (45) is shown in Figure 7(b). The Sequential Impact Law (19) leads to the following post-impact contact velocities

$$\boldsymbol{\gamma}_A^+ = \begin{pmatrix}v & v\end{pmatrix}^{\mathrm{T}}, \qquad \boldsymbol{\gamma}_B^+ = \begin{pmatrix}0 & v\end{pmatrix}^{\mathrm{T}}, \qquad \boldsymbol{\gamma}_C^+ = \begin{pmatrix}0 & 0\end{pmatrix}^{\mathrm{T}}. \tag{46}$$

Using (5), (45), and (46), we obtain

$$\bar{\boldsymbol{\gamma}}_A = \begin{pmatrix}-\frac{v}{2} & v\end{pmatrix}^{\mathrm{T}}, \qquad \bar{\boldsymbol{\gamma}}_B = \begin{pmatrix}-\frac{v}{2} & \frac{v}{2}\end{pmatrix}^{\mathrm{T}}, \qquad \bar{\boldsymbol{\gamma}}_C = \begin{pmatrix}0 & 0\end{pmatrix}^{\mathrm{T}}, \tag{47}$$

and from (6) follows the computation of the impulsive forces for the three impact cases

$$\boldsymbol{\Lambda}_A = \begin{pmatrix}2mv & mv\end{pmatrix}^{\mathrm{T}}, \qquad \boldsymbol{\Lambda}_B = \begin{pmatrix}mv & mv\end{pmatrix}^{\mathrm{T}}, \qquad \boldsymbol{\Lambda}_C = \begin{pmatrix}0 & 0\end{pmatrix}^{\mathrm{T}}. \tag{48}$$

Eq. (47) and (48) allow the evaluation of inequality (18) from Definition 3 for the *ABC*-cycle

$$\boldsymbol{\Lambda}_A^{\mathrm{T}}(\bar{\boldsymbol{\gamma}}_B - \bar{\boldsymbol{\gamma}}_A) + \boldsymbol{\Lambda}_B^{\mathrm{T}}(\bar{\boldsymbol{\gamma}}_C - \bar{\boldsymbol{\gamma}}_B) + \boldsymbol{\Lambda}_C^{\mathrm{T}}(\bar{\boldsymbol{\gamma}}_A - \bar{\boldsymbol{\gamma}}_C) = \frac{-mv^2}{2} \leq 0. \tag{49}$$

Bearing in mind the minus sign from (4), we recognize that (49) is a contradiction to condition (18) from Definition 3. Thus, we can conclude that the set-valued operator $\mathcal{H}$ in (4) is not maximal cyclically monotone for the Sequential Impact Law. Therefore, the Sequential Impact Law cannot be expressed by a convex proper lower semicontinuous dissipation function $\Phi(\bar{\boldsymbol{\gamma}})$.

6 CONCLUSIONS

With the Sequential Impact Law a continuous cone-wise linear impact law has been formulated. It can describe the wave-like phenomena in Newton's cradle and reproduces the experimental observations. Moreover, the Sequential Impact Law is in accordance with the post-impact velocities provided by the one-dimensional wave equation for the collision of three identical thin rods. The Sequential Impact Law is kinematically, kinetically, and energetically consistent. The impact mapping S of the Sequential Impact Law is non-expansive. Accordingly, the corresponding operator $\mathcal{H}$ is maximal monotone. The provided counter-example to maximal cyclical monotonicity lets us conclude that no dissipation function exists for the Sequential Impact Law.

7 ACKNOWLEDGEMENT

This research is supported by the Fonds National de la Recherche, Luxembourg (Project Reference 8864427).

REFERENCES

[1] Ch. Glocker. An Introduction to Impacts. In Nonsmooth Mechanics of Solids, CISM Courses and Lectures, Vol. 485, Springer, Vienna, pp. 45–101, 2006.

[2] R. I. Leine, N. van de Wouw. Stability and Convergence of Mechanical Systems with Unilateral Constraints. Springer, Berlin, 2008.

[3] M. Baumann, R. I. Leine. Convergence based synchronisation of unilaterally constrained multibody systems In Proceedings of the ENOC 2014 Conference, Vienna, 2014.

[4] R. I. Leine, M. Baumann. Variational analysis of inequality impact laws. In Proceedings of the ENOC 2014 Conference, Vienna, 2014.

[5] R. T. Rockafellar, R.-B. Wets. Variational Analysis. Springer, Berlin, 1998.

[6] Ch. Glocker. Energetic consistency conditions for standard impacts Part I: Newton-type inequality impact laws and Kane's example. Multibody System Dynamics, Vol. 29, No. 1, pp. 77–117, 2013.

[7] Ch. Glocker. Energetic consistency conditions for standard impacts Part II: Poisson-type inequality impact laws. Multibody System Dynamics, Vol. 32, No. 4, pp. 445–509, 2014.

[8] K. F. Graff. Wave motion in elastic solids. Clarendon Press, Oxford, 1975.

[9] J. Wittenburg. Schwingungslehre. Springer, Berlin, 1996.